3

Critical Current

3.1 Introduction

By critical current, J_c is meant the maximum lossless current, a superconductor can sustain before the voltage develops.

In general, there can be two contributions to the current flowing on the surface of superconductor. Consider, for example, a superconducting wire along which we are passing a current from some external source. We call this, the transport current (because it transports charge into and out of the wire). If the wire is in an applied magnetic field, screening currents circulate so as to cancel the flux inside. These screening currents are superimposed on the transport current, and at any point, the current density is

$$\vec{J_t} = \vec{J_i} + \vec{J_H}, \tag{3.1}$$

where $\vec{J_t}$ is due to transport current and $\vec{J_H}$ arises form screening current.

The superconductivity breaks (i.e. a resistance appears), if the magnitude of total current density $\vec{J_t}$, at any point, exceeds the critical current density J_c.

If the total current flowing is sufficiently large, the current density at the surface will reach the critical value J_c and the associated magnetic field strength at the surface will have a value H_c. Conversely, a magnetic field of strength H_c at the surface is always associated with a surface super-current density J_c. This leads to the hypothesis:

"A super-current loses its zero resistance at any point on the surface, when the total magnetic field strength, due to transport current and applied magnetic field, exceeds the critical field H_c."

Clearly the stronger the applied magnetic field, the smaller is the critical current. If there is no applied magnetic field, the only magnetic field will be

that generated by any transport current. In that case, the critical current will be that which generates the critical magnetic field H_c at the surface. This special case (of above) is known as *Silsbee*'s *rule*. H_c is known as bulk or thermodynamic critical field.

3.2 Critical Current of a Wire

Consider a long superconducting wire of circular cross-section with radius $a >> \lambda$, carrying a current I. This current produces a circumferential self-field (at the surface) of magnitude

$$H = \frac{2I}{ca}. \tag{3.2}$$

When this field reaches the critical field H_c, it will destroy the superconductivity, which is known as the *Silsbee-criterion*. Thus, the critical current will be

$$I_c = \frac{caH_c}{2}, \tag{3.3}$$

which scales with the perimeter, and not the cross-sectional area of the wire. This current flows in a surface layer of a constant thickness λ. Since the cross-sectional area of this surface layer will be $2\pi a\lambda$, the critical current density will be

$$J_c = \frac{I_c}{2\pi\lambda a} \tag{3.4}$$

$$= \frac{cH_c}{4\pi\lambda} \equiv J_d \text{ (The depairing current density).} \tag{3.5}$$

(The *depairing current density* sets an upper limit to the J_c and is defined by the energy at which super-electrons are excited over the superconducting gap).

The thermodynamic critical field (H_c) for pure element is small (of the order of a few hundred Oersteds). Niobium, Lead or tin are not useful for high field magnets, although zero field J_d is very large. For Pb–Bi alloy, it was found (during 1928) that a field of 25 kOe (2.5 Tesla) was necessary to quench superconductivity. But, a solenoid of this alloy proved disappointing as it did not conduct as expected from Silsbee's rule.

From (3.4), it is seen that the critical current J_c is inversely proportional to the radius of the sample and represents the current at which vortices first enter the sample. The critical current occurs, when the surface field is equal to H_c. This is called *Silsbee*'s *rule*.

Some typical figures for high performance conventional type II superconductors are given in Table 3.1.

The figures in Table 3.1 are to be borne in mind for use of high temperature superconductors in cryogenic technology.

Table 3.1. Critical current and upper critical field

Alloy	J_c	H_{c2}
NbTi	3×10^5 A cm^{-2} at 5 T	11 T (4.2 K) 15 T (0 K)
Nb_3Sn	10^6 A cm^{-2} at 5 T	28 T (0 K)
V_3Ga	2×10^6 A cm^{-2} at 5 T (highest J_c)	–
$PbGd_{0.2}Mo_6S_8$	–	54 T (42 K) 60 T (0 K) (highest)

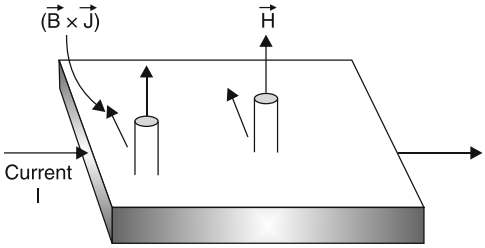

Fig. 3.1. Lorentz driving force acting in a current carrying superconductor in mixed state

3.3 Critical Current in Mixed State

The resistance-less current in a homogeneous type-II superconductor is limited to a value, which just produces field H_{c1} at its surface, as given by Silsbee's rule. Above H_{c1}, the sample contains magnetic vortex lines threading through bulk of the same in the form of a triangular lattice called flux line lattice (FLL).

Now, if we pass a current (called transport current) $\vec{J}$, which is perpendicular to the vortex-cores, a Lorentz driving force equal to $\frac{1}{c}\left(\vec{B} \times \vec{J}\right)$ acts on the vortices, tending them to move. If the vortex lines move in response to the Lorentz force, they will dissipate the energy in the flowing current, specifically the dissipation induces a voltage, and thus, resistance in a sample known as flux-flow resistance (Fig. 3.1).

In a homogeneous wire, there is no counteracting force preventing this. Clearly to carry a large current with resistance, the vortices must be pinned, so that their motion is inhibited there.

3.4 Flux Pinning

If the fluxoid lattice is regular and uniform, the field within the superconductor must also be uniform. From the relation curl $\vec{H} = \mu_0 \vec{J}$, it follows that there cannot be any macroscopic current in the system. Experiments on pure well

annealed samples of type II superconductors show this to be true. Supercurrents can only be made to flow on the surface and resulting critical currents are extremely small. To produce a technologically useful material, which is able to carry macroscopic currents throughout its volume, the distribution of fluxoids must be made non-uniform, so that a finite curl is possible. Then, due to mutually repulsive force between fluxoids, a concentration density gradient will give rise to a net force per unit volume called as driving force given by

$$\left|\vec{F}_{\mathrm{L}}\right| = \frac{B}{\mu_0}\frac{dB}{dx}, \tag{3.6}$$

where B is flux density and $\frac{dB}{dx}$, the gradient. In three dimensions, the relation is

$$\vec{F}_{\mathrm{L}} = \frac{1}{\mu_0}\vec{B} \times \operatorname{curl}\vec{B} = \vec{B} \times \vec{J}\,. \tag{3.7}$$

That is, the force is equivalent to the Lorentz force. To pin the FLL and maintain a current density, the crystal lattice must supply an equal and opposite pinning force per unit volume $\vec{F}_{\mathrm{p}}$. Critical current corresponds to the point, at which the FLL starts to move and we define critical pinning force

$$\vec{F}_{\mathrm{pc}} = \vec{B} \times \vec{J}_{\mathrm{c}} \left(\mathrm{Nm}^{-3}\right). \tag{3.8}$$

Then, flux-pinning is thought to be caused by forces between fluxoids and certain inhomogeneties in the crystal known as *pinning centres*, e.g. if normal core of a fluxoid resides on a small "normal" metal inclusion, its energy will be lowered because there is no longer any need to derive a previously superconducting region normal.

3.4.1 Role of Inhomogeneties

The pinning of FLL can occur through their interaction with various types of microstructural inhomogeneties, such as dislocation networks, different types of inter- and intra-grain boundaries, composition fluctuations, precipitates of a second phases, etc. They give rise to local variations in superconducting properties either through "core interaction" or the "magnetic interaction" with a flux vortex, characterised by normal core radius (ξ) and super-current circulation spread (λ) respectively (generally, magnetic pinning is more important in low k materials).

The interaction between an isolated defect and FLL results in elementary pinning force f_{p}, which when properly summed over all the pinning entities per unit volume, (taking into account the elastic properties of FLL) gives rise to the volume pinning force F_{p}. The critical current, then, is governed by force balance equation

$$\vec{F}_{\mathrm{L}} = \vec{B} \times \vec{J} = -\vec{F}_{\mathrm{p}}\,. \tag{3.9}$$

3.4.2 Flux Pinning (Pinning of Flux-Vortices in Conventional Superconductors)

Two materials, in particular, have been predominantly involved with high field and high current superconducting technology. These are the alloy $Nb_{40}Ti_{60}$ and the compound Nb_3Sn. In the Nb–Ti alloy, flux lines are pinned by tangles of dislocations, which form during drawing of the wire. In Nb_3Sn, the highest critical current is obtained in material with the smallest grain-size, indicating that grain boundaries are the cause of flux pinning. Their metallurgical properties are quite different: the alloy is strong and ductile and can be readily drawn down in large quantities to a diameter of ≈0.2mm, while in contrast, Nb_3Sn is brittle and weak and the fabrication of a conductor in a form suitable for winding into magnet-coils present a number of technical problems. The first superconducting magnets in the 1960s were found to have performances, which were not in accordance with measurements made on short samples of the same wire. A coil would revert to the normal resistive state at a quarter of its expected current value by a process known as quenching. It was recognised that some precautions were necessary to prevent a local quench (caused by a small region of the winding exceeding the critical current density), from propagating and causing a full-scale quench with the possible destruction of the magnet insulation through very large induced voltages. A simple solution to this problem was to clad the superconductor with a low-resistance normal conductor, such as copper. This forms a temporary alternative path for the current in the event of a local resistive region being formed in the superconductor. Composite conductors consisting of strands of superconductor embedded in a matrix of copper have been successfully used for the partial stabilisation of small magnets carrying up to 100 A, but for large magnets, additional cryostatic stabilisation is required. The ratio of copper to superconductor in the windings is greatly increased (∼20:1), and helium is channelled through the winding, so as to be able to remove the heat generated by a local quench, without a catastrophic rise in temperature. The fully stabilised conductors have the disadvantage that J_c reduces to about $10^3\,\mathrm{A\,cm^{-2}}$ (Fig. 3.2).

3.5 Depinning of Flux Vortices

When driving force just exceeds the pinning force, depinning occurs and the current reaches the critical value. Depinning process can be accelerated by thermal activation.

At any finite temperature $T < T_c$, thermal activation added by Lorentz driving force can cause pinned flux lines to hop out of the free energy wells of depth U_0 (the pinning energy) and produce dissipation even when $F_L < F_p$ (Fig. 3.3). This phenomenon is known as *flux creep* (This name is given because of analogous behaviour of dislocations in solids subjected to a load at elevated temperatures).

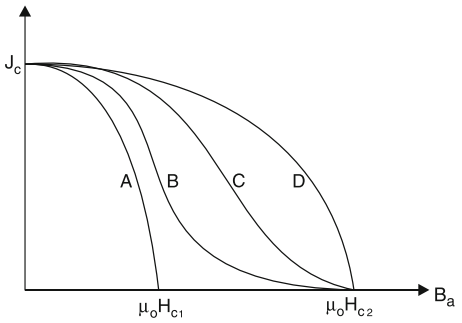

Fig. 3.2. Critical current versus applied field for samples of the same material with increasing amount of flux pinning (from A to D)

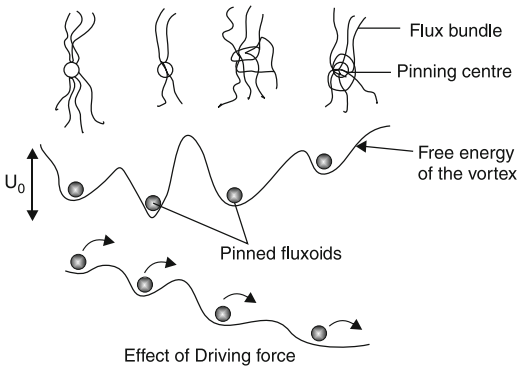

Fig. 3.3. Flux pinning (and depinning) [1, 2]

A pinned vortex has to surmount energy barrier U_0, before it is free to move under Lorentz force. A moving vortex will generate heat until it is trapped at another pinning site. This heating in turn enhances the likelihood that nearby vortices can exceed the activation barrier and the pinning force itself is temperature dependent, leading to a highly nonlinearly coupled system with positive feedback. This thermally activated vortex motion is *flux creep*. As a result, at a relatively lower value of the driving force, depairing effect can become detectable and rate of depairing

$$R = R_0 \exp\left[-\frac{(U_0 - F_{\mathrm{L}} V_x)}{k_{\mathrm{B}} T}\right],$$

$$k_{\mathrm{B}} T \ell n\left(\frac{R_{\mathrm{c}}}{R_0}\right) = -(U_0 - F_{\mathrm{L}} V_x)_{\mathrm{crit}}. \tag{3.10}$$

$$(F_{\mathrm{L}})_{\mathrm{crit}} = \frac{1}{c}\left(\vec{B} \times \vec{J}\right). \tag{3.11}$$

$$(F_{\mathrm{L}})_{\mathrm{crit}} = \left[U_0 - k_{\mathrm{B}} T \ell n\left(\frac{R_0}{R_{\mathrm{c}}}\right)\right] \frac{1}{V_x}. \tag{3.12}$$

R_c is the maximum detectable rate. However, when T is small and U_0 is large, the factor $k_B T\, ln(R_0/R_c)$ is negligibly small and the creep effect is not very important. However, when U_0 is small and T is large, the flux creep can significantly reduce J_c.

3.6 Critical Current in High Temperature Superconductors

Two crucial virtues for the success of Nb–Ti and Nb_3Sn materials are that they develop strong flux pinning and are not granular. The tendency of granular superconductors to subdivide into regions of strong superconductivity separated by weak superconducting interfaces (weak-links) is bad for applications. The critical transport current density (J_{ct}) for transmitting current over useful lengths is then very much less than the local critical current density J_c in the strong superconducting regions with good flux pinning.

In addition to the granular structure, another phenomenon that controls the magnitude of critical current in HTSCs is the flux creep; it is important owing to the possibility of working at quite high temperatures.

3.6.1 Effect of Structure

The first studies on the critical current of sintered HTSCs have brought out some intriguing problems. It was found that

(1) Critical current density given by transport experiments is low and very much magnetic field dependent.
(2) That measured from magnetisation is larger up to a very high magnetic field ($\sim$20 T).
(3) The magnetisation is sample size independent, which is not predicted from Bean theory [3].

The paradoxical data are only consequences of the transport and magnetic measurements not being sensitive to the same contributions: so, the transport current depends chiefly on the current between the grains and, therefore, on the connection between them. It has been shown that in high T_c ceramics, the sintered grain boundary behaves as a weak-link, i.e. as a Josephson junction. So, high T_c superconductors exhibit the behaviour of a granular superconductor. However, the physics of HTSCs is quite different from that of a low T_c superconductor. In low T_c superconductor, grain size is smaller than ξ and λ. In HTSC, the grain sizes are large compared with λ and ξ and so, the high T_c ceramic superconductor has to be understood as a "composite". Clem [2], has proposed that a HTSC can be modelled by considering an array of Josephson junction (JJs) linking grains of type II superconductors. In HTSCs, very rapid flux creep has been reported [4], which is the manifestation of the presence

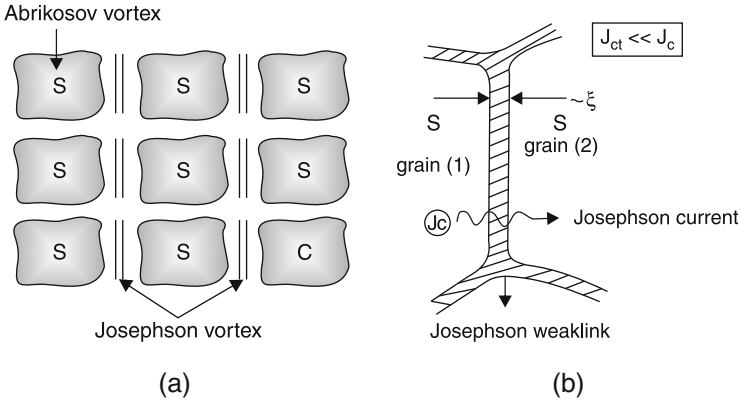

Fig. 3.4. Flux creep model of **(a)** HTSC **(b)** a Josephson junction between two grains

of the Josephson junction array (weak-links), whose activation energy is ϕ_0. However, in the grain and in a single crystal, it has been shown that activation energy is lower than in low T_c superconductors and is magnetic field dependent. Thus, for the temperature range near T_c, the flux creep phenomenon is a major limiting influence on the critical current (Fig. 3.4).

3.7 RSJ Model of an HTSC (High T_c Superconductor)

Unlike conventional (i.e. low T_c) superconductors, grain boundaries play an important role in HTSCs. Due to small coherence length (ξ) and large gap (Δ), the order parameter (therefore, pair potential) is very sensitive to crystallographic defects, particularly grain boundaries.

An HTSC may be viewed to be consisting of strong superconducting grains weakly interconnected by grain-boundaries acting as resistively shunted Josephson junctions (Fig. 3.5).

At 0° K, the inter-grain coupling energy is

$$E_J = \frac{\hbar i(0)}{2e\,\cos\delta}, \tag{3.13}$$

where

$$\hbar = \frac{\hbar}{2\pi} \text{ and } i\,(0) = \frac{\pi\Delta(0)}{2eR_n}. \tag{3.14}$$

R_n is the normal state resistance of the grain boundary.

Equation (3.13) can be written as

$$E_J = \frac{h}{2\pi}\frac{1}{2e}\frac{\pi\Delta(0)}{2e\,R\,\cos\delta} = \frac{h\Delta}{8e^2}\frac{1}{R\,\cos\delta}$$

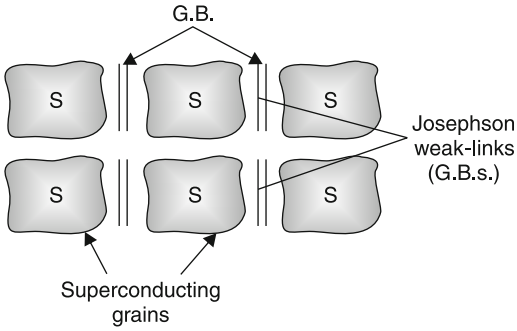

Fig. 3.5. RSJ model of HTSCs

or Josephson coupling energy,

$$E_{\mathrm{J}} = \frac{\Delta R_{\mathrm{Q}}}{2R}, \tag{3.15}$$

where

$$R_{\mathrm{Q}} \equiv \left(\tfrac{h}{2e^2}\right) \Big/ \cos\delta \tag{3.16}$$

is the quantum pair resistance.

At a finite temperature (T), $i(0)$ changes to

$$i_{\mathrm{c}}(T) = \frac{\pi\Delta(T)}{2eR_{\mathrm{n}}} \tan h \left[\frac{\Delta(T)}{2kT}\right]. \tag{3.17}$$

Then

$$E_{\mathrm{J}}(T) = \frac{h\Delta(T)}{8e^2 R_{\mathrm{n}} \cos\delta} \tan h \left(\frac{\Delta(T)}{2kT}\right). \tag{3.18}$$

Here, R_{n} should be small.

In fact, the behaviour of grain boundaries in HTSC is not well described by the Ambegaokar–Baratoff theory due to following three facts:

(1) $I_{\mathrm{c}}\ R_{\mathrm{n}}$ product is $<<\Delta$ (the band gap)
(2) There is anomalous temperature dependence of $I_{\mathrm{c}}\ R_{\mathrm{n}}$ product:

$$I_{\mathrm{c}} R_{\mathrm{n}} \propto (T_{\mathrm{c}} - T)^2$$

(3) $I_{\mathrm{c}}\ R_{\mathrm{n}}$ product is not a constant, but scales with R:

$$I_{\mathrm{c}} R_{\mathrm{n}} \propto \left(\frac{1}{R}\right)$$

Further, $I_{\mathrm{c}}\ R_{\mathrm{n}}(\equiv V_{\mathrm{c}})$ is one- to two-orders of magnitude lower than expected from Ambegaokar–Baratoff relation

$$V_{\mathrm{C}} = \left(\frac{\pi \sqrt{\Delta_1 \Delta_2}}{2e} \right).$$

For granular superconductors, like BSCCO, inter-granular coupling is better modelled as an S–N–S type weak-link than as a tunnel junction, because the short coherence length allows a continuous depression of the superconducting order parameter near the interface connecting two bits of ideal materials. Thus, the Josephson coupling energy E_{j} and the critical current I_{c} are expected, in general, to be less than that implied for the same normal resistance by the ideal Ambegaokar–Baratoff relation (3.18) and (3.17). To get a feel for the numbers, if the inter-granular resistance adds $\sim 10^{-4}\,\Omega{-}\mathrm{cm}$ to the normal resistivity, and if the grain size "a" is $\sim 1\,\mu\mathrm{m}$, it follows that the resistance of a typical inter-granular link is $\sim 1\ \Omega$. For ideal Ambegaokar–Baratoff junctions of YBCO, this would imply a link critical current (at $T = 0$) of $I_{\mathrm{c}}(0) \sim 10^{-2}\mathrm{A}$ or $J_{\mathrm{c}}(0) \sim 10^{6}\,\mathrm{A\,cm^{-2}}$. This value is comparable with J_{c} in crystals, but ceramic samples usually have J_{c} of only 10^{3}–$10^{4}\,\mathrm{A\,cm^{-2}}$, indicating a sizeable reduction below ideal values. Further, if there is a considerable variation in the strength of the Josephson coupling from grain to grain, the properties of the sample may be dominated by relatively few percolating paths of particularly strong junctions.

3.8 Effect of Granularity on Superconductivity

Both nominally uniform and granular thin films tend to lose their zero resistance state at a normal state sheet resistance R_{N}, which is close to the quantum pair resistance.

$$R_{\mathrm{Q}} = \frac{h}{(2e)^2}. \tag{3.19}$$

Uniform films undergo a sharp superconductor to insulator transition near R_{Q}. A truly insulating state is not seen in granular films, until $R_{\mathrm{N}} >> R_{\mathrm{Q}}$.

In contrast to uniform films, the S–I transition in granular films is mediated by a competition between

(1) Grain charging and
(2) Josephson coupling

To put an electron on an isolated grain (of capacitance C), costs an electrostatic energy

$$E_{\mathrm{c}} = \frac{e^2}{2\mathrm{C}}, \tag{3.20}$$

which can become very large, if grains are small. This energy barrier is known as *Coulomb-blockade* and will be detrimental to Josephson (i.e. pair) tunnelling, if E_{c} is comparable to, or large than the Josephson coupling energy E_{J}.

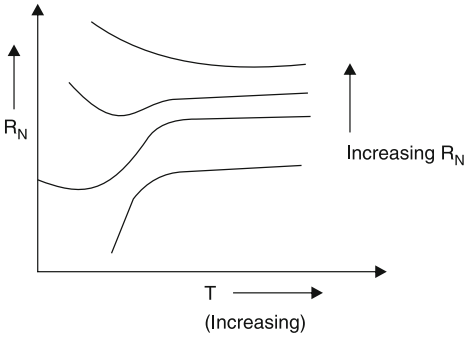

Fig. 3.6. Super-resistive behaviour

Transport properties of the films are dominated by the nature of inter-grain coupling. In low resistance films, $R_N < R_Q$ and "global" superconductivity is established via inter-grain Josephson (i.e. pair) tunnelling. However, as R_N is increased above R_Q, Josephson coupling energy

$$E_J = \Delta\left(\frac{R_Q}{2R_N}\right) = \frac{\Delta h}{8e^2}\left(\frac{1}{R_N}\right) \tag{3.21}$$

becomes small when compared with the characteristic inter-grain dephasing energy E_c and, therefore, the global superconductivity is lost.

At high enough sheet resistance R_N, E_J is diminished to the point that what were formally Josephson junctions become more characteristic of S–I–S tunnel junction with the current being primarily carried via quasi-particle tunnelling. Since the quasi-particle tunnelling is attenuated at temperatures lower than T_c, the film would exhibit quasi-entrance and super-resistive behaviour at $T < T_c$ (Fig. 3.6).

Consider two nearby superconducting grains. Energy cost for a quasi-particle to tunnel from one grain to the other is $(2\Delta + E_c)$, while a Cooper pair tunnelling cost is $4E_c$. Quasi-particle tunnelling will become favourable, if $4E_c > (2\Delta + E_c)$ or if E_c is of the order of Δ.

3.9 Measurement for J_c

High angle grain boundaries reduce the inter-granular transport. After an extensive investigation of various misorientations, the IBM group [5] concluded that all grain boundaries misoriented by greater than 5° are intrinsic weak-links and such junctions are extremely undesirable.

Critical current can be measured in two ways:

(1) Transport current density (J_{ct})

J_{ct} is limited by the weakened properties of the grain boundaries and not by the strong flux pinning properties of the grain interiors. A transport measurement, therefore, represents the lowest value of J_c that can be defined.

(2) Critical current from magnetisation measurements (J_{cm})

The measure of critical current relies on the fact that magnetic moment is equal to the circulating current enclosed into area.

In a granular medium, this can lead to difficulty, because the appropriate area is not the area of the whole sample. Therefore, J_{c} is sometimes insecurely defined.

3.10 Flux Flow and Defining J_{c}

For transport currents above a depinning threshold, the statistically averaged sum of the Lorentz forces on the vortex array exceeds the total pinning force, and therefore, the entire array moves laterally at a steady velocity. This is known as *flux flow*.

The motion of the vortex-lattice results in significantly higher energy dissipation and heat generation by inducing an electromotive force, which drives current through the normal core of the vortex. In a Bardeen–Stephen model, this leads to a velocity dependent force on the vortex.

$$\vec{f}_{\mathrm{v}} = -\eta\,\vec{v}, \tag{3.22}$$

where η is a viscosity coefficient and v is the vortex velocity. Thus, above the depinning current, there is a force balance given by

$$\eta\vec{v} = \vec{f}_{\mathrm{L}} - \vec{f}_{\mathrm{p}}. \tag{3.23}$$

The flux motion produces an electric field

$$E = \eta v\,\phi_0 = vB, \tag{3.24}$$

where B is the average magnetic induction.

Combining these results, a differential flux flow resistivity

$$\rho_{\mathrm{f}} = \frac{dE}{dJ_{\mathrm{T}}} = \frac{\phi_0 B}{\eta}, \tag{3.25}$$

can be defined which can be obtained from the linear portion of I–V characteristic in a field for currents above the depinning current.

For an operational threshold voltage criterion in a transport measurement, the onset of the linear portion of the I–V curve defines J_{c}.

In conventional materials, since $\rho_{\mathrm{creep}} << \rho_{\mathrm{f}}$, establishment of a working criterion for defining J_{c} is not a problem.

A second defining characteristic of flux flow is the scaling of the resistivity ρ_{f} with normal state resistivity ρ_{N} as

$$\frac{\rho_{\mathrm{f}}}{\rho_{\mathrm{N}}} = \frac{H}{H_{\mathrm{c2}}(T)}. \tag{3.26}$$

Because of the high normal state resistivity of the HTSCs, it is clear that there will be substantial energy dissipation at fields H near H_{c2}.

3.11 Anisotropies in High T_c Superconductors

There are various anisotropies in HTSCs. This is shown in carrier concentration. Coherence length $\xi \propto \nu_F$

where Fermi velocity

$$v_F = \frac{\hbar}{n}(3\pi^2 n)^{\frac{1}{3}}, \tag{3.27}$$

$$\frac{\xi_{11}}{\xi_\perp} = \left[\frac{n(11)}{n(\perp)}\right]^{\frac{1}{3}}, \tag{3.28}$$

where ξ_{11} is coherence length parallel to ab plane. $\xi_\perp$ is perpendicular to ab plane.

Experimentally,

$$\frac{\rho_\perp}{\rho_{11}} = \frac{n(11)}{n(\perp)} = 300. \tag{3.29}$$

Therefore,

$$\frac{\xi_{11}}{\xi_\perp} = (300)^{1/3} \approx 6.5, \tag{3.30}$$

$$\left.\begin{array}{r} H_{c2}(11) \propto \left(\frac{1}{\xi_\perp \xi_{11}}\right) \\ H_{c2}(\perp) \propto \left(\frac{1}{\xi_{11}^2}\right) \end{array}\right\} \Rightarrow \frac{H_{c2}(11)}{H_{c2}(\perp)} \propto \frac{\xi_{11}}{\xi_\perp \xi_{11}} \text{ or } \frac{H_{c2}(11)}{H_{c2}(\perp)} = \frac{\xi_{11}}{\xi_\perp} \approx 6.5. \tag{3.31}$$

The Table 3.2 gives the characteristic parameters of Y–Ba–Cu–O compared with some important conventional high field superconductors.

It is clear that a high upper critical field alone is not enough to make the material technologically attractive. Pb Mo_6S_8 did not succeed because of disappointing J_c.

Y–Ba–Cu–O has the highest depairing current density J_d (o). The zero-field J_c values (at 4 K) for thin films are about an order of magnitude close

Table 3.2. Comparison between parameters of conventional and high T_c superconductor Y-Ba-Cu-O

	Nb_3 Ge	$PbMO_6S_8$	$Y_1Ba_2Cu_3O_7$
$\xi(0)$	3,500Å	4,000Å	10–30Å
$\lambda(0)$	35Å	25Å	1,400Å
$H_c(0)$	4 kOe	1.5 kOe	10 kOe
$H_{c2}(0)$	340 kOe	550 kOe	1,200 kOe
$J_d(0)$	8×10^7 A cm^{-2}	3×10^7 A cm^{-2}	6×10^8 A cm^{-2}
J_c(4 K, 0H)	7×10^6 A cm^{-2}	2×10^5 A cm^{-2}	2×10^7 A cm^{-2} (thin film) 2×10^6 cm^{-2} (77 K in thin film)
J_c(4 K, 5 T)	4×10^6 Acm^{-2}	10^4 A cm^{-2}	1.5×10^4 A cm^{-2} (sintered compact)

Table 3.3. FL Lattice melting temperatures of some HTSCs

HTSC	T_c	Lattice melting temperature
YBCO	92 K	75 K
BSCCO	110 K	30 K
TBCCO	125 K	

Table 3.4. Thermodynamic superconducting state parameters of Hg-based superconductors compared with that of YBCO

Quantity/phase	$HgBa_2Ca_{n-1}Cu_nO_{2(n+1)+\delta}$			YBa_2Cu_3
	Hg-1201	Hg-1212	Hg-1223	O_{7-x}
$T_c(K)$	96	127	135	92.2
$\lambda_{ab}(0)$(nm)	268	209	155	89
$\xi_{ab}(0)$Å	21.1	16.6	19.3	16.4
$k_{11c}(0)$ $(=\lambda_{ab}(0)/\xi_{ab}(0))$	127	126	80	74
$(H_{c1})_{11c}$ (0) Oe	123	201	33.5	900
$(H_{c1})_{11c}$ (5 K) Oe	350	320	380	530
$(H_{c2})_{11c}$ (0) Tesla	72	113	88	122
$H_{c(0)} \approx \left[\frac{(H_{c1})_{11c}(0)(H_{c2})_{11c}(0)}{\ell n\ k_{11c}(0)}\right]^{1/2}$ Oe	4,300	6,900	8,200	16,000
$(H_{c2})_{11c}$ (80 K) Tesla	30	68	68	25

to $J_c(0)$. But the sintered compacts have J_c value 2–3 orders of magnitude lower. The highest zero field J_c (at 77 K) of the material sintered and heated above its melting temperature is 7.4×10^3 A cm^{-2} (which is again low) (The bulk single crystals are found to possess J_c values intermediate between thin films and polycrystalline sintered compacts).

Low $J_c(H)$ value suggests that bulk pinning in these materials is low and conventional defects like twin-boundaries, grain boundaries etc. (which although present in abundance) are not providing effective pinning (FLL is extremely stiff and difficult to pin).

Many findings suggest that in sintered compacts, the pinning at $T << T_c$ is provided by inter-grain connections serving as proximity type pinning centres. (The proximity connections are in the dirty-limit). The number of effective pinning proximity centres increases with decreasing temperature. At T close to T_c, current is essentially weak-link like. The exponential decrease of J_c with H reported for some bulk and thin film specimens is indicative of dominance of surface pinning and near absence of bulk pinning. In suitably oriented films containing field H_0, where J_0 is high and is much less sensitive to J_c, the effect is attributed to a larger coherence length ξ_{11} in ab plane along which the current flows and, therefore, inter-grain weak-links are not so effective. J_c is, therefore, no longer strongly sensitive to imposed field and high J_c values upto 1.5 T could either be due to strong surface pinning effect or favourably aligned

defects like twin boundaries or grain boundaries providing more effective bulk pinning.

For low temperature superconductors, FLL melting temperature is well above the critical temperature. So FLL melting does not affect superconductivity.

It should be noted that flux pinning is a complex and imperfectly understood field of study. The details are extremely sensitive to the particular material and its defect population.

When the defects range from the visible (e.g. grain boundaries, twin boundaries, dislocations, voids and particles of second phase) to the invisible (e.g. cation disorder or oxygen vacancies), it is not surprising that there is a little agreement on what determines flux pinning.

It is to be noted here that Bi-and Tl-based materials are not likely to be useful at liquid N2 temperatures in applications that demand a magnetic field, unless in some way pinning is provided. Many of the projected applications involve magnetic fields, therefore, the Y:123 compounds (with even their lower T_c but higher lattice melting temperature) become the material of choice for many uses.

3.12 Flux Pinning in High Temperature Superconductors-

Any spatial variation in H_{c2} or k (the GL parameter) will produce a binding energy δE between a fluxoid and the defect, which is given by

$$\delta E = \int \mu_0 H_c^2 \left(-\frac{\delta H_{c2}}{H_{c2}} |\psi|^2 + \frac{1}{2} \frac{\delta k}{k^2} |\psi|^4 \right) dv, \tag{3.32}$$

where H_c is the thermodynamic critical field that defines the superconducting condensation energy $U_0 = 1/2\mu_0 H_c^2$. v is the volume of the pinning reaction and ψ is the order parameter.

HTSCs exhibit flux creep much more strongly than older superconducting materials. The basic phenomenon underlying flux creep is the thermal activation of fluxons out of their pinning wells (U_0) at a rate proportional to exp $(-U_0/k_B T)$. The maximum well depth is obtained when fluxoid cores find normal regions, because, then the entire condensation energy $1/2\mu_0 H_c^2 v$ is saved. One may expect U_0 to be large, because of the higher critical fields than LTSCs, but coherence length is also much smaller. This implies that the interaction volume is low. Since T_c is high, and temperature enters exponentially in the Boltzmann factor for thermal activation of fluxons, therefore, even a small increase in U can enormously reduce the creep rate.

On one hand, if the defects are small (of the order of ξ), this will favour a high J_c. On the other hand, if the defects are $>\xi$, the superconductivity will be locally disrupted. One of the key goals is to engineer pinning centres that

are extended in one- or two-dimensions so that their increased volume can make U bigger, however, without inducing granularity or decreasing the pin density too much. This implies that flux creep effects can be reduced through addition of appropriate defects, which should be small when compared to coherence length and not too abundant, otherwise, they will reduce T_c and also not too few, otherwise there may be significant motion of the vortices leading to lower J_c.

3.13 Columnar Defects and Flux Pinning

The laminar character of the high T_c cuprates dictates that they can pin the vortices only in the form of pancakes rather than as infinite cylinders perpendicular to the CuO_2 layers (Fig. 3.7).

As a result, these materials define an *irreversibility line* that demarks the boundary between two regions in the mixed state zone of the B–T plane: (a) In the region of low magnetic field B and low temperatures T (no flux flow), the electric current can flow without energy dissipation. In this region, T_c is non-zero and magnetisation is irreversible.

(b) At large B and T (the second region), the flux is staggering and any current will dissipate energy. In this region, the critical temperature vanishes and magnetisation behaviour is reversible.

The reversibility line is lower in BSCCO than in YBCO. This implies that BSCCO is more anisotropic and consequently planes are less coupled in BSCCO.

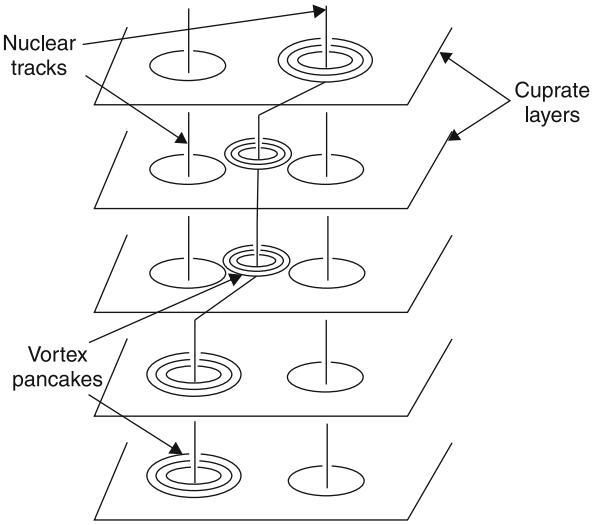

Fig. 3.7. Flux pinning in the form of pancakes

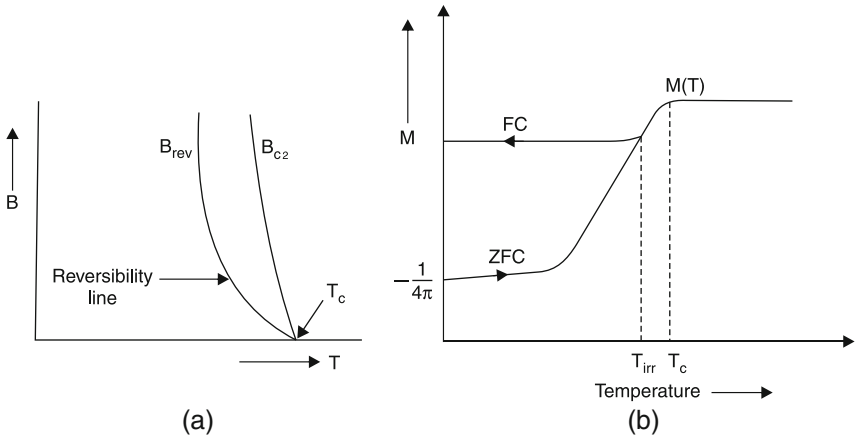

Fig. 3.8. (a) (B, T) diagram for a high T_c superconductor. **(b)** Magnetic moment versus temperature

Figure 3.8b depicts magnetic moment as a function of temperature. After being cooled in zero field (ZFC), M vs. T is measured in a field $H > H_{c1}$ with increasing temperature. Then, $M = -1/(4\pi)$ (or less) is obtained at low temperature and $M(T)$ as indicated. If the sample is cooled in a field (FC), then different $M(T)$ is obtained.

Below T_c, there is a temperature T_{irr}, where $M(T)$ of the ZFC and FC results are the same. These measurements can be performed for different magnetic fields and $T_{irr}(H)$ determined. The line of $T_{irr}(H)$ in the H–T plane is called the irreversibility line. Above and to the right of this line, the sample has reversible magnetic behaviour. Below and to the left of this line, the sample has irreversible behaviour (Fig. 3.8a).

3.13.1 Flux Pinning in HTSCs by Vortex Pancakes

The common feature of HTSCs is the presence of double/triple layers of CuO_2 planes, which are believed to be the superconducting planes. The coherence length along the planes is <2 nm. In case of YBCO, this leads to the weak-link problem, probably because T_c of this material decreases considerably with oxygen deficiency, which especially occurs at grain boundaries. The distance between the superconducting layers is relatively large and is responsible for the large, to very large anisotropy of the superconducting parameters. Consequently, the pinning in these materials is also very anisotropic, partially because

$$F_p \propto B_{c2}^n (T)\, b^p (1-b)^q$$

and

$$B_{c211} >> B_{c2_\perp}, (b = B/B_a),$$

but also because of the very anisotropic nature of the vortex lattice itself.

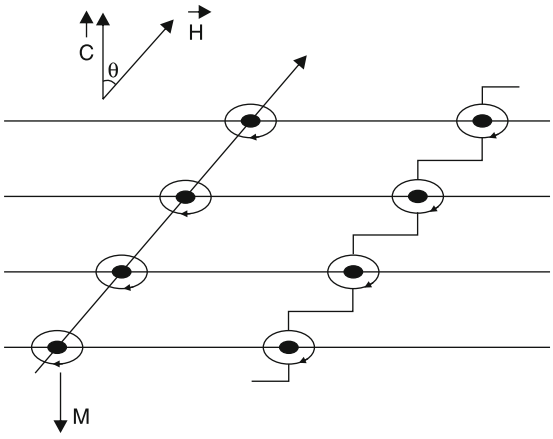

Fig. 3.9. Schematic view of two representations of flux lines intersecting CuO_2 double layers. (*Horizontal lines*) when the field $\vec{H}$ makes an angle θ with the c-axis

When the decoupling between the layers is large (as in Bi-and Tl- compounds), the super-currents are confined to the layers and the vortices are segmented into vortex-pancakes with weak electromagnetic and Josephson coupling between them. This is demonstrated in Fig. 3.9, where two different representations are given for a flux-line in an applied field making an angle θ with the normal to the superconducting layers (c-axis).

In Fig. 3.9, the ellipses lying in the *ab* plane depict superconducting screening current. To the left, is the continuous flux line picture for very anisotropic superconductor, to the right, the segmented flux-line picture with pancake vortices valid for Josephson coupled superconducting layers. (Note that the magnetisation is directed along the c-axis). The segmentation is indicated by current loops in the CuO_2 (i.e. *ab*) planes. The magnetic moment related with the screening current is oriented along the normal, which leads to a net torque on the sample when θ deviates from either $\theta = 0$ or $\theta = \pi/2$. This provides an accurate way to measure the anisotropy parameter. The zeros of the order parameter and the vortex cores are depicted by black dots. The representation at left shows the vortex in the anisotropic 3D picture, while the zigzag line at right represents the vortex in the quasi-2D case (The latter applies below the cross-over temperature). The vortex consists of 2D pancake vortices in the layers and Josephson vortices along the layers. Flux-line cutting in such a system leads to quasi-2D behaviour above a cross-over field B_{2D} defined by

$$B_{2D} = \frac{\varphi_0}{t_a s^2},$$

where t_a = anisotropy parameter and s = entropy density

For Bi = 2212, $B_{2D} \approx 0.3\,\mathrm{T}$

and for Tl:2212, $B_{2D} \approx 10\,\mathrm{mT}$
(according to $s \approx 1.5\,\mathrm{nm}$ and $t_a = 3 \times 10^3$ and 10^5 respectively).

In many respects, the properties of the vortex lattice for $B > B_{2D}$ may be considered as if a thin superconducting film of thickness s in a perpendicular field is studied.

The different behaviour of J_c in Y:123 and Bi:2212 is caused by the large difference in anisotropy of both materials [6, 7].

Magnetisation experiments have shown that the anisotropy of J_c and irreversible magnetic field (B_{c2}) of the BSCCO system is much larger than that of the YBCO system. J_c decreases drastically, when the magnetic field deviates from the *ab*-plane for a YBCO thin film. A *c*-axis oriented BSCCO thin film has a strongly enhanced J_c, when the field is parallel to *ab*-plane. For the Tl films at 77 K, it has been found that when B is parallel to *ab* plane, the J_c values are 1.2×10^4 and $1.5 \times 10^3\,\mathrm{A\,cm^{-2}}$ at 5 tesla and 16 tesla, respectively. However, when B is perpendicular to *ab* plane, J_c decreases drastically to $1.3 \times 10^3\,\mathrm{A\,cm^{-2}}$ at 0.7 tesla. This anisotropy of J_c indicates the existence of strong pinning centers parallel to the *ab*-plane, which could be explained using the intrinsic pinning model proposed by Tachiki and Takahashi [8]. The structure of Tl:2223 is composed of CuO_2 layers (superconductive) and other layers (Tl–O double layers), which are weakly superconductive or insulators. Then, the weakly superconductive or insulator layers work as strong pinning centers for flux lines parallel to the layers.

3.14 Experimental Results on Introduction of Flux Pinning Centers in HTSCs

In 1991, by scanning tunnelling microscopy, it was discovered at Los Alamos and IBM Ruschlikon that in epitaxial films there were large number of screw dislocations $\left(\approx 10^9/\mathrm{cm}^2\right)$ much more than in substrate ($SrTiO_3$). This led to an understanding that these screw dislocations may pin the vortices leading to large critical currents.

Subsequently, we will consider results on

(1) Melt textured growth
(2) Chemical inhomogenity (in the form of precipitates of second phase)
(3) Production of extended defects (columnar defects) by (1) heavy ion beam or (2) neutron irradiation.

3.14.1 Melt Textured Growth

A significant improvement in J_c of YBCO ceramic has been obtained by radical change in the processing method. Instead of conventional solid phase sintering, the technique involves partial or complete melting and controlled solidification. This results in a dense material with a microstructure consisting

of locally aligned, high aspect ratio grains with short dimensions ∼2–5 μm. The short grain axis is parallel to the c-axis. Adjacent grains are only slightly misoriented with respect to each other (low angle grain boundaries predominate). Due to slow cooling of the melt, a platelet morphology is obtained. That is, in melt textured growth, two dimensional structure of YBCO favours its oriented growth in two specific crystal directions (a and b), thus, avoiding the formation of boundaries in the copper layers.

One may think of melt textured growth method as a compromise between chemistry aimed at producing perfect single phase sample of Y:123 and ceramic processing aimed at making a perfect ceramic without cracks. This method has been extensively developed using either a thermal (temperature) gradient [9, 10] or more recently, a magnetic field gradient [11].

3.14.2 Introduction of Second Phase (Chemical Inhomogeneity)

Murakami and his colleagues at ISTEC in Tokyo [12] have been very successful in strengthening the flux pinning of melt-processed YBCO by introducing progressively smaller (∼0.1 μm) insulating Y_2BaCuO_5 particles as pinning sites. The particles are still large by fluxoid diameter standards. The ISTEC group has succeeded in raising J_c (77 K), pushing the irreversibility line to higher fields and reducing the flux creep rate.

3.14.3 Extended Defects (Columnar Defects)

In 1989, Bernard Raveau and his colleagues, began bombarding samples of YBCO with heavy ions to enhance flux pinning by creating extended defects. Others undertook studies with heavy ion beams [13] and neutron irradiation [14]. The advantage of high energy heavy ions over other modes of irradiation is that, they create amorphous columnar defects of widths comparable to the coherence length in the copper layers (nuclear track is generated by bombarding with 5.3 GeV Pb ions coming perpendicular to copper layers). The structure of such tracks consist of an almost amorphous region forming a cylinder of 7 nm diameter (which is ≈ the vortex core radius). Thus, energetic heavy ions are efficient projectiles for modifying and tailoring the superconducting properties of high T_c cuprates. They generate columnar defects perpendicular to the copper layers that act as efficient flux pinning centres provided that ion species, its energy and the beam fluence are carefully chosen. Such extended defects play a crucial role in controlling the magnetic hysterisis and, thus, give huge enhancement of J_c.

3.15 Magnetic Phase Diagrams of HTSCs

Figure 3.10 compares the magnetic phase diagrams of a conventional type II superconductor and a high temperature superconductor.

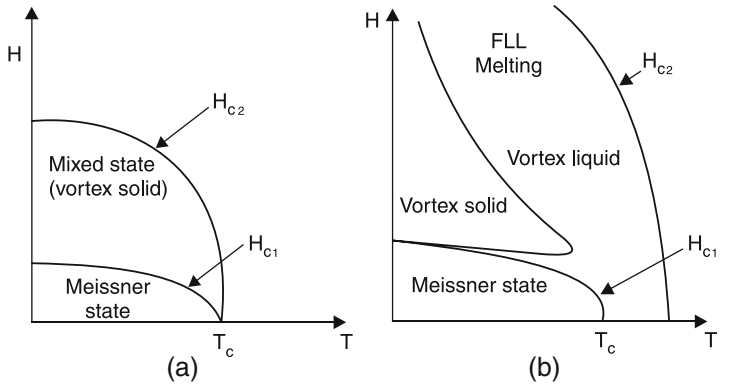

Fig. 3.10. Magnetic phase diagram of **(a)** conventional (type-II) superconductor and **(b)** an HTSC

It has been suggested by Mathew Fisher (a theorist at IBM) that if there are enough pinning defects (centres) in the material, the superconductor may arrange itself into a vortex-glass state, in which the flux vortices do not move, i.e. there is no flux creep (converse of lattice melting).

For HTSC, the vortex solid is either a lattice (FLL for clean superconductors) or a (vortex) glass (for "dirty" superconductors). At Bell communications Research, Steve Gregory and Charles Rogers have done sensitive "vibrating reed" experiments, in which a thin film of superconductor is mechanically vibrated in a magnetic field and observed as oscillations die out. These experiments imply that superconducting films were in a vortex glass state. They interpret the state as arising from an entanglement of the flux lattice lines (FLL). If the lines were flexible enough, they may twist around each other like a tangled pile of spaghetti. This tangling may then allow the entire flux lattice to be pinned with many fewer defects than would be necessary, if the lines were free of each other (as if in lattice) (Fig. 3.11).

In absence of thermal fluctuations, the upper critical field for a type-II superconductor is given by

$$H_{c2} = \frac{\phi_0}{2\pi\xi^2}. \tag{3.33}$$

Thus, small coherence length for HTSCs should give rise to large H_{c2} ($\sim$100 T). In presence of thermal fluctuations, the temperatures are higher. Consequently, energies to create and move vortices are lower.

Energy for movement is determined by temperature and energy to create vortices is determined by field (and therefore ξ and λ). The relevant energy scale is that required to create a piece of vortex line, whose length is ξ (i.e. one coherence length). So this energy $\sim(\xi/\lambda^2)$ is much lower for HTSCs (because of small ξ and large λ). Smaller coherence length and large penetration lengths reflect that density of (mobile) pairs is relatively low.

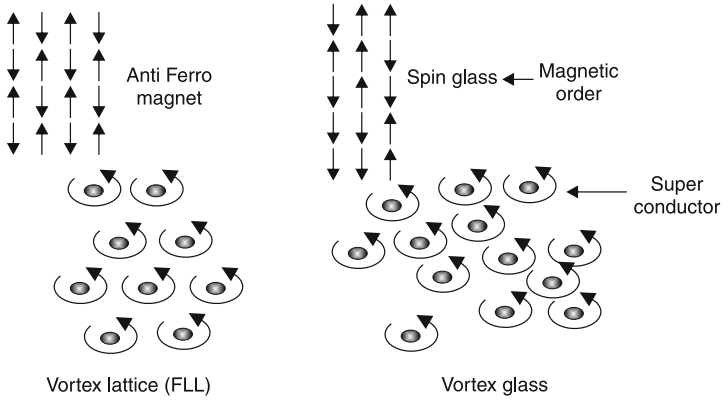

Fig. 3.11. Magnetic order versus superconductor analogy

The effects of enhanced thermal fluctuations are found in presence of an applied magnetic field. It is marked by the presence of vortex-liquid regime between the H_{C2} (T) and the vortex solid phase in the phase diagram.

On cooling, in a field $H < H_{c2}$, the electrons start to pair up and vortices form in the pair wave function near H_{c2}. In the vortex-liquid state, vortices are mobile and have only short-range correlations in their positions, like atoms in a conventional fluid. This regime extends to lower temperature in more and extremely anisotropic HTSCs (like BSCCO), particularly when the applied magnetic field is directed perpendicular to the Cu–O_2 layers. In this case, the vortex lines actually consist of strings of "points" or "pancake" vortices in each superconducting Cu–O_2 layer with only weak correlations between pancake vortices of different layers.

It has been found for BSCCO that in fields $\geq$5 T, it does not become a better conductor than copper even upto 30 K, inspite of the expectation that its resistivity should have vanished at a temperature $T_c\,(H_2) = 80$ K. This fact is explained quite naturally by the large vortex-liquid regime in case of BSCCO. It is a natural analogue of the disordered paramagnetic phase of magnetic materials, when heated above the Curie (or Neel) temperature. Vortex motion scrambles the phase of the pair wave function disrupting any possible long-range coherence ($\rightarrow$no superconductivity).

3.16 Melting of the FLL Because of Reduced Size of $\xi_{GL}(T)$

For $T << T_c$, $\xi_{GL}(T)$ is between 0.5 and 30 Å. At $T \leq T_c$.

$$\xi_{GL}\,(T) = \xi_{GL}\,(0)/(1 - T/T_c)^{1/2}\,, \tag{3.34}$$

since $\xi_{GL}(T)$ is $<< \lambda_L$ (type II superconductor).

So, we have extremely high low-temperature value for H_{c2}. Associated with the short ξ is weak pinning of fluxoids compared with the pinning in

the conventional superconductors. This decreased flux pinning diminishes the size of J_c.

3.16.1 Effect of Reduced Size of $\xi_{GL}(T)$

As the sample is warmed up, the shear modulus of the fluxoid lattice goes to zero at a temperature below T_c. This melting may account for an upward curvature (i.e. a positive second derivative) in the graph of the $B(T)$ curve at which electrical resistance appears.

Although the flux pinning is weak at temperatures comparable with T_c, it is large enough at lower temperatures to make measurements of the H_{c1} very difficult (Values in literature for H_{c1} of Y:123, e.g. range from 1 to 5,000 Oe).

Flux pinning is responsible for the measured magnetic susceptibility being different, when measured on a sample cooled in a constant magnetic field than on one cooled in a zero field, and exposed to field after the lowest temperature is reached. In the former case, the fluxoids move out of the sample as it is cooled, whereas in the latter, they move into it as it is heated; in each case, flux pinning impedes the motion. These two types of data are frequently referred to as "Meissner data" and "Zero field-cooled data" respectively.

3.17 Kosterlitz–Thouless–Berezinski Transition

If the superconductor-film thickness is comparable to the coherence length, then at any finite temperature (even at zero field) there are vortices present in the film. Because energy necessary to create a vortex is very small if the length of a vortex is less than the coherence length, therefore, there is always a significant number of thermally excited vortices in very thin films, and there is also an equal number of anti-vortices, so that there is no net field at any significant distance from film. Thus, in addition to Cooper-pairing, another phase transition occurs due to pairing of vortices and anti-vortices, which is complete at a temperature represented as T_{2D}. (T_{2D} is $< T_{c(0)}$). (This effect has also been observed in two-dimensional helium films). $T_{c(0)}$ is the bulk transition temperature. This two-dimensional transition to zero resistance in films occurs at a temperature below the bulk transition temperature of the parent material. The difference ($T_{c(0)}$–T_{2D}) is proportional to the sheet resistance of the 2D film.

For T_{2D} to be closer to $T_{c(0)}$, the sheet resistance should be low. At T_{2D}, there would be a sharp increase in superfluid density, and this would manifest itself in any property sensitive to n_s (e.g. kinetic inductance). If, either the thin film is granular or has a low carrier concentration, the T_{2D} will be significantly different from $T_{c(0)}$, because of large sheet resistance.

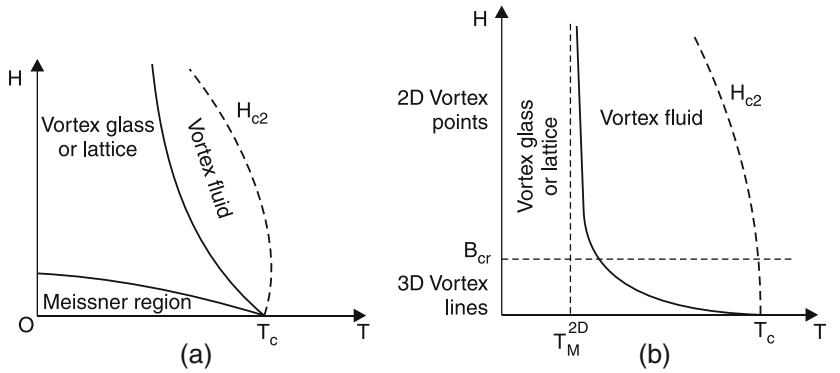

Fig. 3.12. Schematic phase diagram for melting of FL solid for **(a)** YBCO and **(b)** BSCCO

This vortex pairing transition implies reduced dissipation. To study this transition, granular films are nice, because of lesser pinning than homogenous films.

3.18 Anisotropy and Change Over from a 2D to 3D Behaviour

For highly anisotropic Bi-and Tl- based compounds (in the absence of external magnetic field), the superconducting transition corresponds closely to the Kosterlitz–Thouless transition for 2D systems. Thermal fluctuations are very important in HTSCs. In applied magnetic fields, thermal fluctuations modify the field-temperature (i.e. B–T) phase diagram with respect to the mean field one, which is dependent on anisotropy also.

The layered structure of the materials leads to the existence of a critical value for the magnetic induction B_{cr} which separates regions of 2D and 3D behaviour of the vortex system and hence, different regimes of vortex-lattice melting.

Figure 3.12 compares the phase diagrams for melting of the flux line solid for a 3D material YBCO with that of a highly layered material BSCCO. The results for BSCCO are with $\vec{B} \parallel \vec{c}$. The melting line starts near T_{c}, rising initially as $(T_{\mathrm{c}}–T)^2$ until B_{m} reaches a value B_{cr} at $T \sim T_{\mathrm{m}}^{\mathrm{2D}}$, after which B_{m} rises almost vertically.

Figure 3.12 shows the contrasting behaviour of the two HTSCs. It is to be mentioned here that the melting temperature $T_{\mathrm{m}}^{\mathrm{2D}}$ (which marks the cross-over flux density B_{cr} for BSCCO) is at inaccessibly high fields for the 3D material YBCO.

3.18.1 High Field Regime ($B >> B_{cr}$)

The interaction energy between 2D vortices in the same layer is stronger than the interaction energy between vortices which belong to different layers. This results in a quasi-2D behaviour of the vortex system, which can be considered as made of only weakly interacting 2D vortex lattices in different layers. In this case, the melting temperature is close to the strictly 2D (Kosterlitz–Thouless) melting temperature, which is field independent.

$$T_m^{2D} = \left(\frac{A}{8\pi\sqrt{3}}\right)\left[\frac{d\varphi_0^2}{(4\pi\lambda_{ab})^2}\right] \tag{3.35}$$

$(A \approx 1)$
where $d =$ inter-planar distance
$\varphi_0 =$ flux quantum
$\lambda_{ab} =$ in plane component of London penetration depth.

For Bi:2212, the above equation gives

$$T_{\mathrm{m}}^{2D} \approx 25{-}30 \text{ K}$$

in real systems. In presence of field

$$T_{\mathrm{m}}(B) = T_{\mathrm{m}}^{2D}\left[1 + \frac{b}{\ell n^{2.70}\left(\frac{B}{B_{\mathrm{cr}}}\right)}\right], \tag{3.36}$$

where b is a constant ($\approx$1).

3.18.2 Weak Field Region ($B << B_{cr}$)

The relative displacement of 2D vortices in adjacent layers is much smaller than the displacement due to fluctuations (disorder) and the vortex-lattice follows a 3D behaviour. In this case,

$$T_{\mathrm{m}}(B) = \left(\frac{c_{\mathrm{L}}^2}{2^{3/2}}\right)\frac{d\varphi_0^2}{(4\pi\lambda_{ab})^2}\left(\frac{B_{\mathrm{cr}}}{B}\right)^{\frac{1}{2}}, \tag{3.37}$$

where $0.1 \geq c_{\mathrm{L}} \leq 0.4$.

$T_{\mathrm{m}}(B)$ in this equation indicates the melting temperature from a 3D vortex lattice to a liquid of 3D vortex lines. A further increase of temperature results in dissociation of vortex lines into 2D vortices which are free to move independently in each layer at a temperature

$$T'(B) = T_{\mathrm{m}}(B)\left(\frac{B_{\mathrm{cr}}}{B}\right)^{\frac{1}{2}} (> T_{\mathrm{m}}(B)). \tag{3.38}$$

3.18.3 The Cross-Over Field B_{cr}

Average inter-vortex distance in the plane is

$$\approx \left(\frac{\varphi_0}{B}\right)^{\frac{1}{2}} \tag{3.39}$$

and Josephson length

$$= (\gamma d) \tag{3.40}$$

where anisotropy parameter

$$\gamma = \left(\frac{\lambda_c}{\lambda_{ab}}\right). \tag{3.41}$$

λ_c is out of plane penetration length, d is the inter-plane distance. This implies

$$B_{\mathrm{cr}} \approx \frac{\varphi_0}{(\gamma d)^2} \tag{3.42}$$

The behaviour of real materials is very sensitive to anisotropy: the parameter γ in Bi:2212 depends on the oxygen content, for a fixed value of the reduced temperature $t = (t/T_{\mathrm{co}})$, J_{c} is found to increase with increasing oxygen content. This effect can be explained with the reduction of effective anisotropy (γ) and, therefore, with a more 3D character of vortex fluctuations in oxidised samples.

3.19 The Effect of Anisotropy Parameter γ on the Vortex Phase Transitions

An increase of γ results in decrease of B_{cr} $\left(\sim 1/\gamma^2\right)$. This implies melting temperature of the vortex lattice decrease with decrease in oxygen content, for a

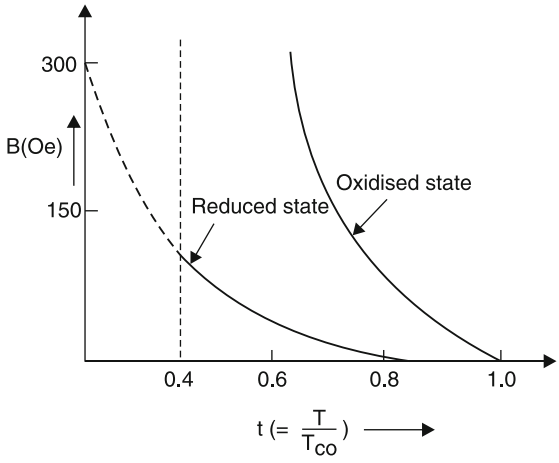

Fig. 3.13. Behaviour of magnetic irreversibility line for two different oxidation states of BSCCO film

fixed value of the applied field. In strongly reduced samples, the cross-over field can be so close to H_{c1} that (3.37 and 3.38) would have no temperature range of validity. Figure 3.13 shows the behaviour of the magnetic irreversibility line for two different oxidation states of BSCCO film.

The B_{cr} values were found to be ∼1,000 and 100G, respectively for oxidised and reduced states. Such changes in B_{cr} correspond to a large variation of the anisotropy parameter γ (from 80 to 300 respectively).

The transition temperature to the vortex glass phase (T_g), decreases as the anisotropy factor γ increases reaching $T_g = 0$ at $\gamma = \infty$ (pure 2D). In the presence of finite inter-layer coupling, the 2D vortex glass correlation length grows resulting in a transition to 3D vortex glass phase at sufficiently low temperatures $T_g \sim (1/\gamma^n)\,(n > 0)$.

3.20 Desired Microstructure Synthesis for High Critical Current Density in High T_c Superconductors

3.20.1 Some Inherent Problems (Weak-Links and "Flux Lattice Melting")

When the initial euphoria regarding the discovery of HTSCs subsided, and attempts regarding the deployment of HTSCs in devices started, it became evident that certain practical problems will have to be solved. One of the major (practical) problem relates to the low critical current density (with or without applied magnetic field) for the as synthesised HTSC materials. The lower value of critical current densities arises due to both inter-grain (weak-link) and intra-grain (flux lattice melting) effects. There have been speculations that the above effects are inherent in certain specific properties of HTSC materials, including those very properties that are thought to be responsible for making the new oxide superconductor as HTSCs, for example the HTSCs are known to have lower carrier densities as compared to the low T_c metallic superconductors (LTSCs). In the new oxide cuprate superconductors, according to one popular view, the charge carriers are provided by deviating the nominal valence of copper from 2^+ to $(2+\delta)^+$ where $0 < \delta < 1$. The materials, which contain divalent copper ions are insulators, despite the odd number of valence electrons expected per unit cell. The genesis of gap-formation in the conduction band is thought to be due to strong electron correlation relative to the energy corresponding to the band width. For those compositions (n_s), where superconductivity sets in, it has been known that the energy gap structure is essentially retained on doping of the carriers to a substantially high level. However, if the doping level is increased, the carrier density could be increased further, but then, the gap seems to get destroyed. The transition temperature then decreases rapidly. Because of this, the maximum useful carrier density remains in the range $\sim 2 \times 10^{21} - 5 \times 10^{21}\,\mathrm{cm}^{-3}$. This value is substantially (about 100 times) lower than that obtained for conventional

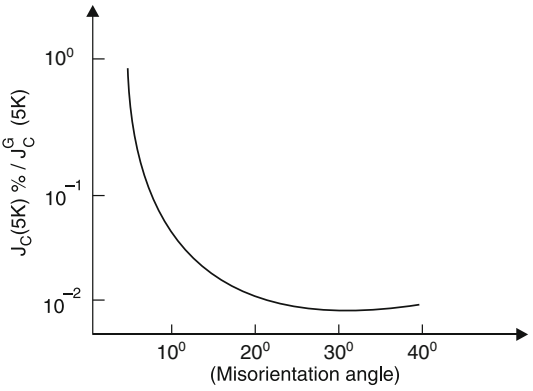

Fig. 3.14. Ratio of critical current density (grain boundary J_c) to the average value of current density J_c^G in the two adjacent grains as a function of the misorinetation angle in the basal plane

superconductors. It is, therefore, apparent that low carrier density is native to HTSC materials. However, this low carrier density leads to several undesirable aspects regarding the application potential of HTSCs. One important effect of low carrier density is that it leads to a potential barrier at the grain boundary, which hinders the transmission of the electrical current across the grain boundary (GB). [15] were the first to outline the presence of potential barrier at the boundary. In a more recent study, the transport critical current (inter-grain) has been found to get reduced to varying degrees depending on the relative tilt angle between the boundaries (Fig. 3.14) [16].

Another problem related with current transport is due to flux lattice melting. This again is related to the inherent properties of HTSCs. This relates to coherence length ξ, which has its origin in the finite distribution range of momentum of the electronic states resulting in the formation of Cooper-pairs. The coherence length can be approximated as $\xi = n' v_F / (\pi\Delta)$, where ν_F is the Fermi velocity, Δ, the superconducting gap and n' the carrier density. For the case of a low carrier density material, the Fermi sphere and hence, Fermi velocity is small. The superconducting gap Δ is range in the high T_c materials (since Δ is an increasing function of T_c). In view of their large Δ and small ν_F, it is unlikely that the new materials will possess large coherence lengths. It has been estimated that for Y-123, $\xi_{ab} \cong 30\,\text{Å}$ and $\xi_c \cong 3\,\text{Å}$ and for $Bi_2Sr_2CaCu_2O_8$, $\xi_{ab} \cong 35\,\text{Å}$ and $\xi_c \cong 3\,\text{Å}$. It may be noted that for conventional superconductors, e.g. for Nb, $\xi \cong 400\,\text{Å}$. The small coherence length leads to small pinning force and hence this limits the intra-grain critical current. One possible simple way of looking at this problem is as follows: A pinning centre has an effective dimension $\sim\xi$. The energy to destroy superconductivity, i.e. the condensation energy is $H_c^2/(8\pi)$ per unit volume. Thus, if we have a non-superconducting precipitate of volume ξ^3, an excess energy of $\xi^3 H_c^2/(8\pi)$ is required to push a flux line out of the precipitate [17]. The

value of H_c is larger for HTSCs (e.g. 3 T for Y:123) than for conventional superconductors (e.g. for Nb, it is ∼0.2 T) However, for HTSCs, the value of ξ^3 is much smaller. For example in cuprate HTSCs, it is 5×10^{-27} m^3 (vs 6×10^{-23} m^3 for Nb). As a result, pinning energy in cuprate HTSC is smaller than in conventional superconductor by a factor of 10^3. The pinning energy for YBCO, derived on the basis of these arguments, is 0.04 eV (It may be pointed out that the thermal energy at 77 K is 0.006 eV). Thus, the pinning energies are not large enough to circumvent the thermally activated depinning. As a consequence, a finite resistivity would be expected in a magnetic field even at very low current level.

In addition to the aforementioned inter-grain weak-link and intra-grain flux-lattice melting problems, yet another factor that limits the current carrying capacity of HTSCs is their anisotropy. The best current capacities are observed for current flow in the a–b plane, and poorer in the c-axis direction. The improvements to raise the capacity in this regard do not seem feasible. Thus, in the subsequent discussion, we would confine ourselves to discuss possible ways out of the "weak-link" and "flux-lattice melting".

3.20.2 Possible Ways Out of "Weak-Links"

As described previously, the weak-links correspond to grain-boundaries. Since the first forms of HTSC materials produced were polycrystalline pellets, the weak-link problems were invariably present and the transport current (across the GBs) was very low (∼10 A cm^{-2}). One easy way out of the weak-link effects could be found in the earlier works on metals and alloys and also on some inorganic solids, where material forms were produced from polycrystalline

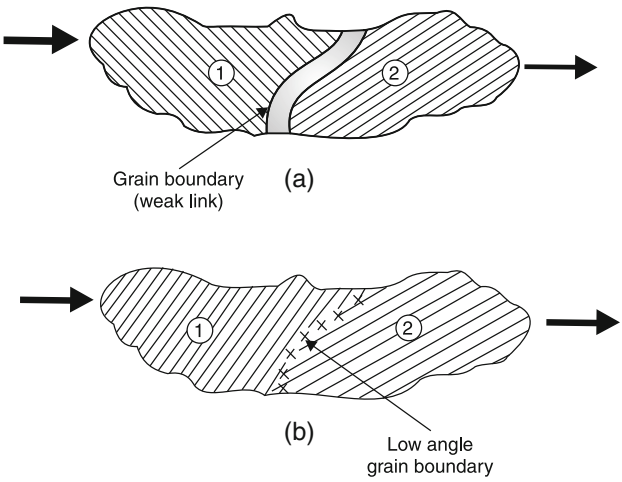

Fig. 3.15. The passage of current across **(a)** high angle and **(b)** low angle grain boundary. In case of former, there is a large but for the latter, very small decrement in current

versions through a process termed as "texturing". In this, the crystallites of the polycrystalline forms were provided treatments so that they adopt specific orientations, and hence, would be separated (generally) by low angle grain boundaries (Fig. 3.15). For instance, it has been reported that the diminution in critical current decreases as the misorientation between grains decreases [18], i.e. as high angle grain boundaries yield to give rise to low angle boundaries. Thus, when electrical current passes through a polycrystalline configuration with low angle grain boundaries, the diminution in it is minimum. Thus, if texturing is imparted through a suitable process, the critical current density would get significantly enhanced, e.g. under suitable conditions, it may reach upto $\sim 10^5$ to $\sim 10^6\,\mathrm{A\,cm^{-2}}$. It is interesting to note that the first reports of higher J_c ($\sim 10^5\,\mathrm{A\,cm^{-2}}$) were for thin films deposited on suitable substrates, as for instance, for $YBa_2Cu_3O_{7-\delta}$, the substrates employed corresponded to MgO, ZrO_2 and $SrTiO_3$ [18]. Considerations of thin film formation on these substrates held at elevated temperatures (300–500°C) would reveal that they nearly satisfy the conditions of epitaxial growth in thin films. Without going into details, it may be pointed out that in this growth process, the depositing atoms/molecules lead to formation of crystal like regions, which nearly adopt the substrate crystal orientations (Fig. 3.16). Thus, in thin films, texturing is automatically provided during the film formation.

On one hand, texturing leads to similar effects in thin films and bulk, for the former, it gets naturally imparted during film formation process itself. On the other hand, for bulk, texturing has to be necessarily done after synthesis (growth) of the initial material. Being a post-synthesis process, it corresponds to an additional process step. Also, an HTSC being a multi-component material, imparting texturing is rather an involved process. Because of these factors, texturing in bulk has not yet been a routine step, although several specific texturing processes have been put forward. Out of the various texturing processes developed so far, those which seem to be important are those

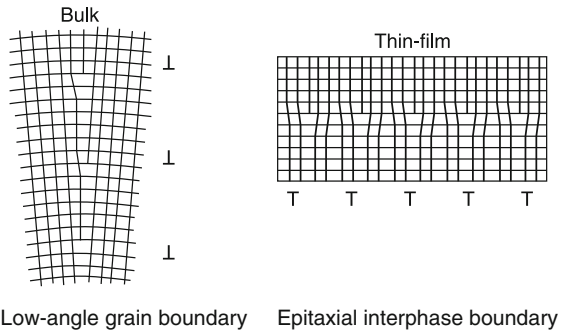

Fig. 3.16. Low angle and epitaxial inter-phase boundaries resulting due to texturing

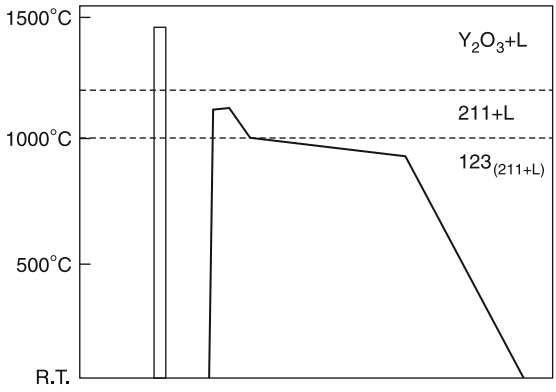

Fig. 3.17. Phase diagram illustrating QMG process

proposed by Murakami [19], and a more recent process – the so called "continuous" process proposed by Professor Paul Chu's group at Houston (Meng et al. Nature **34**, 326 (1990)). These processes are briefly discussed in the following, with emphasis on embodied principles.

The texturing process propounded by Murakani et al. is essentially a quench melt growth (QMG) process, which leads to

(1) Suppression of the second phase intrusions
(2) Improvement in the connectivity of the superconducting phase and
(3) Grain alignment

and thereby, the achievement of high J_c in the Y–Ba–Cu–O system. The QMG process can be described with the help of the diagram shown in (Fig. 3.17).

The QMG process is based on the known phase transformations in Y:123 material. Some salient features can be recapitulated. When the 123 bulk precursor cools from a single phase liquid region to 1,050°C, it undergoes the transition

$(Y_2O_3 + \text{liquid}) \rightarrow (Y_2BaCuO_5 + \text{liquid}) \rightarrow (123 + \text{liquid of composition } BaCuO_2 + CuO)$.

At around 1,050°C, 123 forms through a peritectic solidification according to Y_2BaCuO_5 + liquid $(3BaCuO_2 + 2CuO) \rightarrow 2YBa_2Cu_3O_{6.5}$. Now, if the material is heated above the solidus temperatures (1,020–1,200°C), it helps to dissolve the impurity phases, which are precipitated in the grain boundaries. In addition to this, crystal grains grow more easily in a liquid solution. Thus, the QMG texturing process consists of rapidly heating 123 above the solidus temperature (or even above the melting point) and then, slowly cooling through the peritectic temperature.

In the QMG process, first a stoichiometric $YBa_2Cu_3O_7$ pellet is heated to 1,450°C for a few seconds, and then it is quenched to room temperature. This step creates precursor material consisting of fine Y_2O_3 particles scattered through out liquid phases of copper oxide and barium copper oxide. Then, the

precursor material is heated to 1,100°C for 20 min. This causes the Y_2O_3 particles to react with the liquid, forming a fine and homogeneously dispersed 2–1–1 phase. The material is cooled to room temperature. This causes the 2–1–1 phase to react with the liquid phases, creating a well connected 1–2–3 microstructure. Cooling of the material in a temperature gradient encourages directional growth of $YBa_2Cu_3O_7$ phase. The cooling should be done in flowing oxygen, so that enough oxygen can be incorporated to induce the tetragonal to orthorhombic transition. It is also possible to incorporate oxygen into the sample by post-annealing at around 600°C after fast cooling from 900 to 950°C, where the growth of the 123 phase terminates.

The above QMG process leads to alignment of grains and hence, is like a texturing process, which creates material having grains aligned within few degrees. This Murakami's process leads to textured HTSC materials with very high J_c and was verified by Salama [20], who obtained a current density of 37,000 A cm^{-2} in a magnetic field of 0.6 T.

More recently, a continuous bulk HTSC texturing process has been developed by Prof. Paul Chu's group at Houston [21]. These investigators, to allow the continuous growth of large samples of bulk 123 that are capable of carrying a high J_c and to help remove impurities, moved the 123 bulk precursor through an open tubular furnace having a pre-set temperature profile that includes a narrow hot zone (Fig. 3.18). Meng et al. have set the temperature profile in accordance with the known phase transformation in 123 material, which has already been described while dealing with Murakami process.

The temperatures are $T_1 = 500 \pm 25$°C. The time spent in different zones are: 1 (not critical); 2: (10 ± 5 min); 3: (100 ± 50 h); 4: (20 ± 5 h). The peritectic temperature is 1,050°C [21].

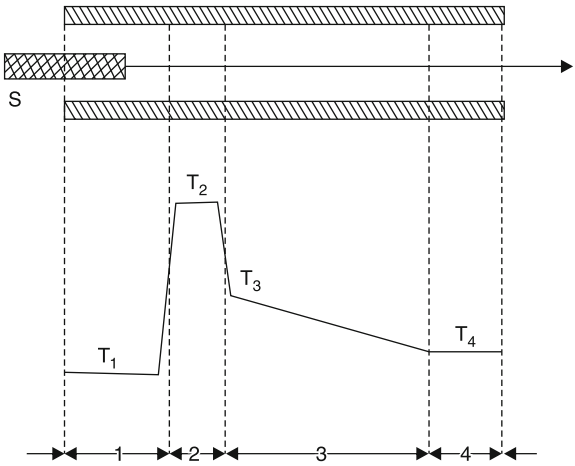

Fig. 3.18. Illustration of continuous process for step (3) in the preparation of bulk 123 sample (S)

They have varied both the speed $\mathrm{d}x/\mathrm{d}t$ and the gradient $\mathrm{d}T/\mathrm{d}x$, to give the desired rate of temperature change $\mathrm{d}T/\mathrm{d}t$. Meng et al. sintered a bar of dimensions $5.2 \times 0.5 \times 0.3\,\mathrm{cm}^3$ from a 123 fine powder precursor at 940–960°C for 24 h in an oxygen atmosphere to obtain 90% of the theoretical density of $6.3\,\mathrm{g\,cm}^{-3}$. The bar was heated to 1,100°C very rapidly for a short time, before it was cooled rapidly to near the peritectic temperature (∼1,050°C).

The specimen was then made to go through peritectic solidification very slowly. Due to narrow hot zone, zone refining occurs along the axis of travel depositing Y_2BaCuO_5 at one end of some of the samples. Small pieces from different parts of the bar were oxygenated at 500°C for 24–48 h. The resulting bar has very good grain alignment throughout the bar. This was confirmed by scanning electron microscopy and X-ray diffraction techniques. The XRD of the samples taken through the texture processing as per the details suggested by Meng et al., clearly shows that the a–b plane coincides with the longitudinal fracture face along the direction of travel and that all of these planes in the sample are parallel to each other. Some typical J_c values obtained by Meng et al. at 77 K can be outlined here. For a sample of dimensions $1 \times 0.04 \times 0.05$ cm was $2 \times 10^4\,\mathrm{A\,cm}^{-2}$ at 0 T, $1.1 \times 10\,\mathrm{A\,cm}^{-2}$ at 0.54 T and $7.5 \times 10^3\,\mathrm{A\,cm}^{-2}$ at 0.82 T. For the case of the applied field parallel to J_c, J_c was found to be about $1.4 \times 10^4\,\mathrm{A\,cm}^{-2}$ at 0.82 T. This clearly suggests that weak-links get largely eliminated in the texture processing carried out by Meng et al.'s process.

One significant advantage of Meng et al.'s texturing process is that it has continuous nature. Therefore, practical forms like plates, rods, ribbons and perhaps thick films can be fabricated from bulk superconductors having practical forms. The processing of the bulk 123 within the framework of Meng et al.'s process can be divided into four steps (1) the synthesis of powder precursor, (2) sintering of bulk precursor, (3) melt-textured growth and (4) oxygenation. By employing proper temperature gradients and speeds in different zones of the furnace, steps (2) and (4) can be combined into a single continuous process. Another modification, which can be done is the lowering of processing temperature. This can be done by using low melting flux comprising of $BaCuO_2$ and/or CuO and a more reducing atmosphere or halogen. This may be particularly useful for HTSC wires or ribbons, which may involve metal cladding, e.g. silver sheath.

It appears, at present, that the HTSC materials prepared by Meng et al.'s process may be somewhat inferior to that of Murakami's quench melt growth process in regard to the critical current density. However, Murakarni et al.'s process is a batch process, whereas the Meng et al.'s is a continuous process, which is of a great advantage.

3.20.3 Provision of Flux Pinning Sites

Even when the weak-links are taken care of through texturing, the flux lattice melting problem still remains and the critical current density in the magnetic

field undergoes significant diminution due to flux disordering. As discussed previously, to circumvent flux disordering problem, the microstructure has to be suitably tailormade. If the microstructure contains no defects i.e. the crystal is perfect, it would not sustain any current. It is only when defects get created that a current would be -carried through. This is so since the defects can pin the flux and hence it would not disorder and disappear. This is so because the Lorentz force between the transport current and the flux lines causes the latter to move. A voltage is thus created unless the flux lines are pinned. The defects are really the glue which keeps the lattice together and without them, there would be no transport current. The defects must be of the order of coherence length (i.e. $\sim$30 Å for *ab* plane in YBCO). Thus effective flux pinning centres would correspond to localised defects with dimensions of few times the coherence length.

The "flux lattice melting" achieved serious attention after the appearance of the article "Superconductivity: Is the party over" by Robert Pool [22] where he described the work of several investigators including David Bishop of AT and T Bell labs and brought out the limitations on J_c arising from flux lattice melting into sharp focus. The flux lattice melting has been dramatically demonstrated by D. Bishop [23] by comparing the electron micrograph of the flux lattices (revealed indirectly by magnetic particles attracted towards the ends of flux lines) of Y- and Bi-bearing HTSC materials. According to Bishop, the flux lattice in YBCO melts at about 75 K and that in BSCCO, around 30 K. The ways and means of circumventing the flux lattice melting have been extensively explored. It appears that one of the effective ways to arrest the flux lattice melting is to tailor-make the HTSC materials so that they contain a second phase in the form of fine particles which are constrained to the dimensions of the coherence length. It may be found that this can be obtained by suitably adjusting melting and quenching process in the QMG (Murakami) or continuous (Chu) texturing processes. The processes of using a liquid phase in the peritectic region naturally produces second phase materials. Adjustments of quenching conditions may produce second phase particles with dimensions constrained to the dimension of coherence length. The HTSC material in such cases i.e. when QMG or continuous growth also produces second phase flux pinning centers, will have truly large J_c, since in such material forms, weak-link problem has been taken care of by texturing and FLL melting has been arrested by the second phase particles (e.g. 211 particles in the textured 123 material obtained through QMG).

In 1989, it has been shown that irradiation of 123 HTSC material with fast neutrons ($\sim$1 MeV) also leads to enhancement of intra-grain critical current density by as much as hundredfold [24]. The enhancement in the fast neutron irradiated ($\sim$1 MeV, fluence $7.9 \times 10^{16}\,\mathrm{cm}^{-2}$) 123 HTSC results due to creation of neutron irradiation induced defects which act as pinning centres. There have been several other results on the neutron irradiation induced enhancement of intra-grain critical current density J_c [24]. However in none of

these investigations the nature of defects created by fast neutron irradiation has been elucidated. Janam et al. [25] made investigations on unravelling the defects created through neutron irradiation. The 123 single crystals grown by flux ($BaCO_3$ and CuO) method were tested for superconductivity ($T_c \sim 85$ to 90 K). These crystals were then irradiated with 1 MeV neutrons (fluence $10^{16}\,cm^{-2}$) at Dhruva reactor of Bhabha Atomic Research Centre, Mumbai. The defects created by neutron Irradiation were explored by transmission electron microscopy. TEM bright field micrograph revealed that the defects consist of linear spikes (Thermal spikes of width ∼100 Å). At later stages, the spike becomes displacement spike. Both the thermal spike (∼100 Å) and displacement spike defect clusters (∼300 Å) have dimensions ∼3 to 10 times the coherence length ($\xi_{ab} \sim 30$ Å). It is these defects which correspond to flux pinning centres and seem to be responsible for the enhancement of a critical current density on fast neutron irradiation of 123 HTSC single crystal [24].

3.20.4 Desired Microstructure for High J_c

From the preceding discussion, it is clear that for the viable optimum high critical current across the inter-grain (weak-link) and also intra-grain (flux lattice melting) will have to be optimised. Thus processes leading to texturing and provision of "flux pinning centres" both will have to be carried out before the new cuprate HTSC becomes a potentially viable practical material at least for the majority of more useful applications, where high critical transport currents are desired. It appears that for specialised applications, thin film forms where texturing automatically takes place, will continue to find favoured position. Here the flux pinning centres will have to be provided either through the provision of fine aggregates of a second phase or through localised defects created e.g. by neutron irradiation. An interesting aspect of the HTSC thin films is that not only texturing gets automatically imparted but due to different energetics prevalent during their formation, some non-equilibrium and/or metastable second phases (e.g. 211 in aY:123 matrix) gets formed. These phases may serve as flux pinning centres. Thus the thin films may represent desirable forms where with a little effort one can get high critical current density. However, for many general application bulk HTSC forms will be needed. Here, additional processes will have to be carried out so that the as synthesis material becomes a viable form capable of high critical current density. Based on the present state of the art, it appears that first a texturing like Murakami "QMG" or Chu "Continuous" process will have to be carried out so as to eliminate or decrease the density of weak-link. This will have to be followed by a process aimed at providing flux pinning centres e.g. second phase precipitation or defect creation through fast neutron irradiation. A schematic plan for achieving the special microstructures with textured grains and with local second phase/defect cluster configurations is shown in Fig. 3.19.

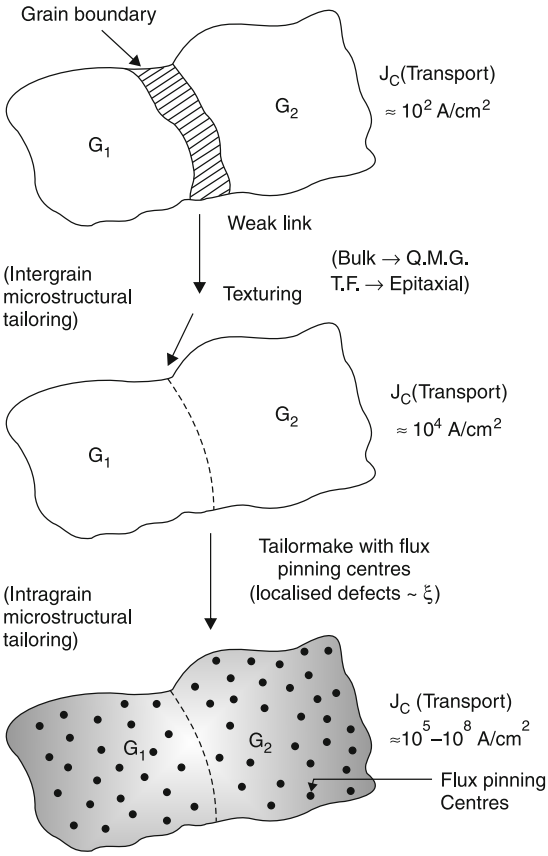

Fig. 3.19. A schematic plan for developing high critical current density bulk HTSC (After: Prof. O.N. Srivastava, Banaras Hindu University, Varanasi, India)

3.21 High T_c Technology

A recent study by the US department of Energy and the Electric Power Research Institute offers a detailed survey of the potential applications of high temperature superconductors once J_{ct} reaches $10^5 A/cm^2$. The survey predicts extensive markets for HTSCs in electric motors, power electronics, transportation, heat pumps, electromagnetic pumps and materials production. These application offer the long term prospect of reducing our total energy consumption by ∼3%. At liquid He temperatures, the critical current of the new materials (BSCCO) exceeds $10^5 A/cm^2$ in a 25-tesla field, besting the Nb based superconductors in their temperature regime. These results have been

obtained on tapes with a high degree of crystallographic alignment, produced by repeated cycles of sintering and mechanical deformation.

Until now, Nb-Ti or Nb_3Sn have been used for very-high field magnets. The present record is 20T for powered magnets and 15 T for persistent current NMR magnets. BSCCO superconductors have the potential to function in fields exceeding 20T. A second advantage of BSCCO materials is that their critical currents vary little with temperature in the range 4–20 K. This suggests an extensive market for magnets that can be cooled by cryocoolers without requiring immersion in liquid helium such cryocoolers work very comfortably in the range 10–20 K without Joule-Thompson expansion values. Sato's Sumitomo team have already constructed a small BSCCO wire solenoid that generates 0.9 T at 4.2 K and 0.1 T at 77 K. It seems likely that we will soon see commercial superconducting magnets with cryocoolers. At liquid nitrogen temperatures, the best results for BSCCO have not yet reached 10^5 A/cm^2. The maximum critical current at 77 K are about 5×10^4 A/cm^2 at zero field and $1 \times 10^4/cm^2$ at 1 T. [26]. However the general conclusion about the long term potential of the BSCCO (and TBCCO) materials at 77 K are not yet justified because these compounds cannot maintain strong flux pinning at temperatures above 30 K because of strong flux creep and FLL melting. At the same time, the much lower anisotropy of Y-123 superconductors and their better flux creep properties at present justify, for many, a continued push to understand and defeat the weak-link problem posed by the grain boundaries in the Y123 compounds.

3.21.1 Advantage of Weak Pinning

The weak pinning behaviour is advantageous for making devices where free flux motion is required, for example a dc transformer. A dc transformer consists of two magnetically coupled but electrically isolated granular films. By passing a dc current in film A, the vortices will move (due to Lorentz force). The vortices in film B will also move. Moving vortices always produce a voltage (and a current). So, there will be an induced dc current in film B just by passing a current in film A.

3.22 Comparison Between Non-Uniform Order in a Solid and that in a Superconductor

We know that in a crystalline solid, the order parameter is the atomic position, while in the superconductor; it is the pair centre-of-mass phase. The table compares some special cases of non uniform order in the two cases.

Solid	Superconductor
1. *Screw dislocation in a solid* The order advances by one lattice spacing in going around the dislocation line.	1. *Vortex-line in a superconductors* The pair-phase advances by 2π in going around the vortex core.
2. *Slip-plane in a solid* The atomic spacing is shifted Δa	2. *Superconducting tunnel junction* The pair-phase difference is between the two superconductors
3. In the solid, the inter-atomic forces are short range implying that low lying order fluctuation modes are phonons	3. The corresponding fluctuations of the phases in the superconductor involve fluctuations in charge density and the long-range coulomb forces give them the plasmon energy in a bulk superconductor. (-Anderson)
4. A solid near its melting point	4. In 3-D, the thermal excitation of phase fluctuation modes can lead to the disintegration of the phase ordering below the "bulk" transition temperature determined by the quasi-particle excitations (i.e. melting of FLL (flux line lattice))

References

1. A.V. Narlikar, *in Critical Current and Vortex Pinning in (high temperature) Superconductors*, ed. by S.V. Subramanyam, E.S.R. Gopal, High Temperature Superconductors. (Wiley, New York, 1989)
2. J.R. Clem, Physica **C 50**, 153 (1988)
3. C.P. Bean, Phys. Rev. Lett. **8**, 250 (1962)
4. Y. Yeshurum, A.P. Malozemoff, Phys. Rev. Lett. **60**, 2202 (1988)
5. D. Dimos, P. Chaudhuri, J. Manhart, Phys. Rev. **B 41**, 4038 (1990)
6. T.T.M. Palstra et al., Phys. Rev. **B 41**, 6021 (1990)
7. T.T.M. Palstra et al., Phys. Rev. **B. 43**, 3756 (1991)
8. Tachiki and Takahashi, Solid State Commun. **72**, 1083 (1989)
9. S. Jin et al., Appl. Phys. Lett. **52**, 2074 (1988)
10. S. Jin et al., Appl. Phys. Lett. **54**, 584 (1988)
11. R. De Rango et al., Nature **349**, 770 (1991)
12. M. Murakami et al., IEEE Trans. Mag. **27**, 1479 (1991)
13. W.K. Chu et al., Nucl. Instr. Methods B **59–60**, 1409 (1991)
14. H. Weber et al., in *Studies of High Temperature Superconductors*, vol. 9, ed. by A.V. Narlikar (Nova Science, NY, 1991), p. 37
15. Y. Enomoto et al., Jpn. J. Appl. Phys. **20**, L 661 (1981)
16. D. Dimos et al., Phys. Rev. Lett. **61**, 219 (1988)
17. K. Kitazawa, Cer. Bull. **68**, 880 (1889)
18. P. Chaudhuri et al., Phys. Rev. Lett. **58**, 2687 (1987)

19. M. Murakami et al. Jpn. J. Appl. Phys. **28**, 1189, (1989)
20. K. Salama et al., Appl. Phys. Lett. **54**, 2352 (1989)
21. R.L. Meng et al., Nature **34**, 326 (1990)
22. R. Pool, Science **244**, 914 (1989)
23. D. Bishop, in *International Conference on Superconductivity*, Bangalore, Jan 1990
24. R.B. Van Dover et al., Nature **342**, 55 (1989)
25. R. Janam et al., Solid State Commun. (1990)
26. K. Sato et al., IEEE Trans. Mag. **27**, 1231 (1991)